Electronic Supplementary Material (ESI) for Journal of Materials Chemistry C.

Supporting Information

Multilevel Nonvolatile Visible Light Photomemory Based on Charge Transfer in Conformal Zinc-Tin Oxide/Au Nanoparticle Heterostructure

*Li-Chung Shih, Sheng-Rong Lin, Rajneesh Chaurasiya, Po-Yen Kung, Song-Syun Jhang, Bernard Haochih Liu, Yen-Hsun Su, and Jen-Sue Chen**

L. C. Shih, S. R. Lin, Dr. R. Chaurasiya, Dr. P. Y. Kung, S. S. Jhang, Prof. B. H. Liu, Prof. Y. H. Su, Prof. J. S. Chen

Department of Materials Science and Engineering

National Cheng Kung University

Tainan 70101, Taiwan

E-mail: jenschen@ncku.edu.tw

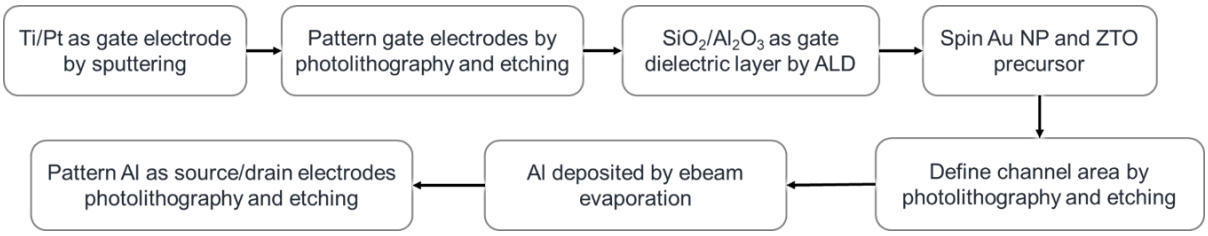

Figure S1. The process flow of ZTO/Au NP photomemory large area array. First, Ti/Pt as a gate electrode is deposited on a substrate by sputtering and patterned through the photolithography and etching processes. As a gate insulator, SiO_2 or Al_2O_3 can be deposited by the atomic layer deposition (ALD). The thickness and quality of gate insulator are crucial to prevent the leakage current of ZTO/Au NP photomemory. Subsequently, the Au NPs precursor is spin-coated on the gate insulator, followed by the spin-coated ZTO active layer. The photolithography and etching processes are again needed to define the channel area. Finally, Al can be deposited via the electron beam evaporation, and then patterned again by photolithography and etching processes to define the source and drain electrodes.

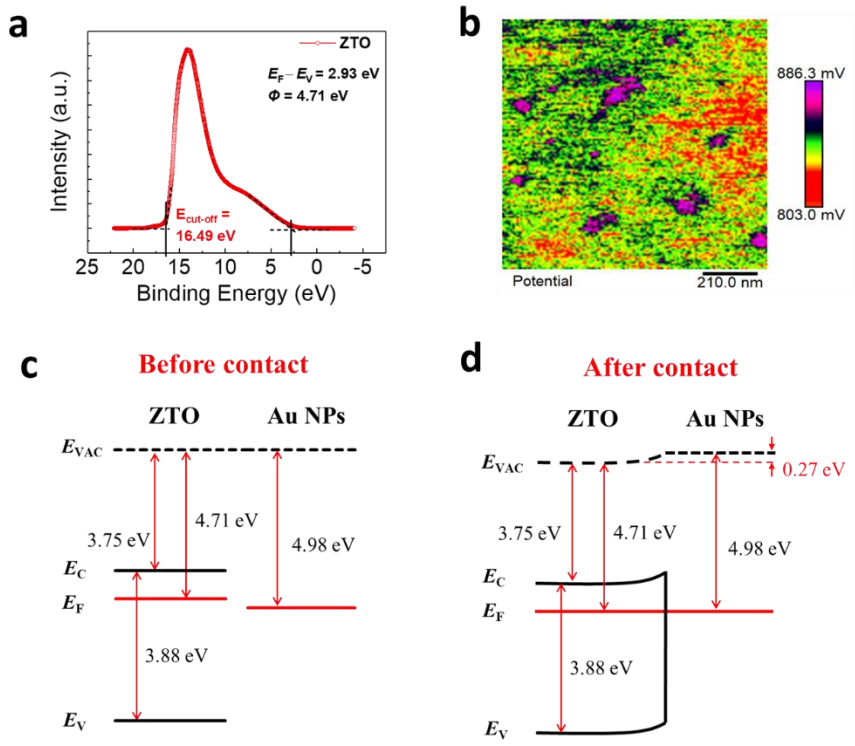

Figure S2. Band diagram analysis of ZTO and Au NP. a) UPS spectrum of ZTO. b) the constant potential difference (CPD) image of Au NPs on SiO_2/p^+-Si substrate from KPFM. The work function of Au NPs is calculated to 4.98 eV. Thermal equilibrium band diagram of ZTO and Au NPs c) before and d) after contact.

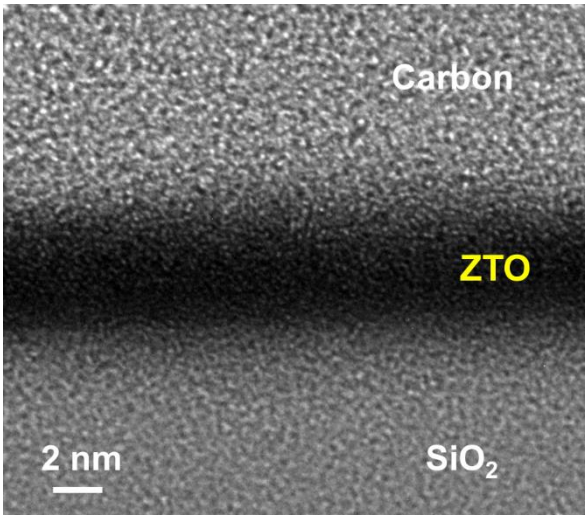

Figure S3. High resolution cross-sectional TEM image of spin-coated ZTO on a SiO_2/p^+-Si substrate.

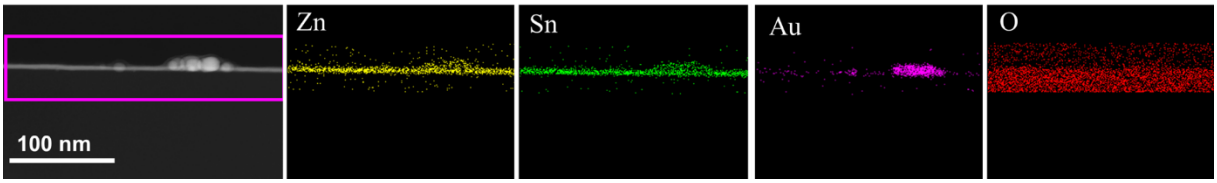

Figure S4. The EDS elemental mapping analysis of ZTO/Au NP heterostructure.

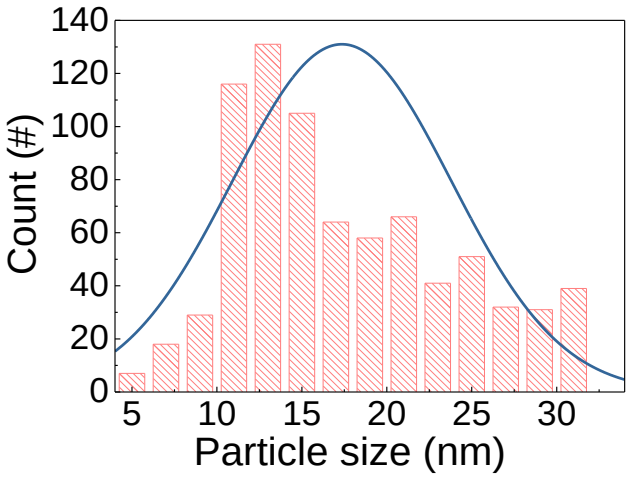

Figure S5. The Au NPs size distribution histogram.

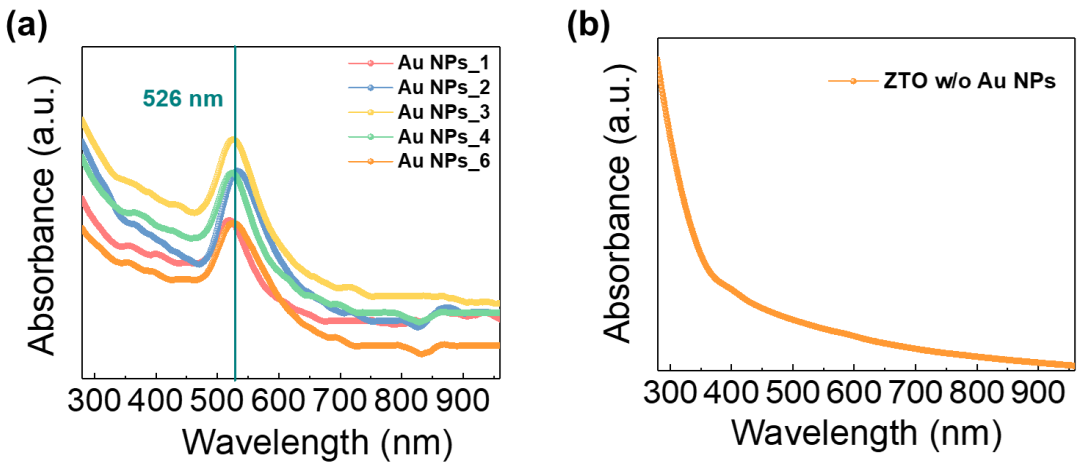

Figure S6. a) The absorption spectra of the Au NPs of six different samples. b) The absorption spectrum of ZTO without Au NPs.

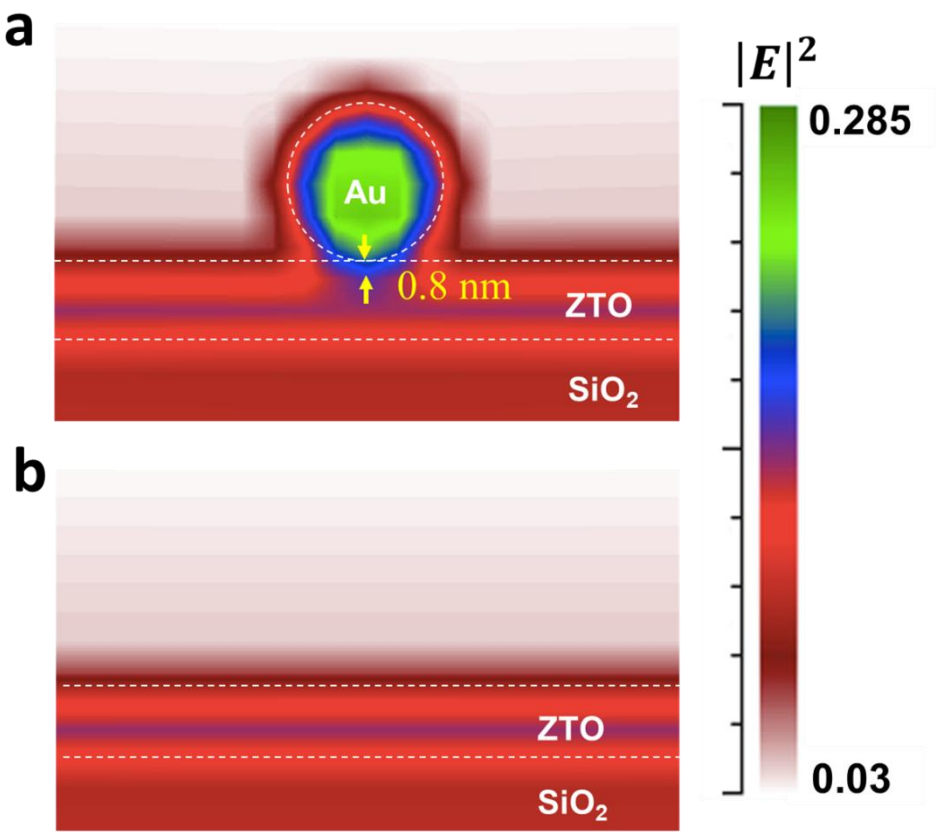

Figure S7. The simulated electric field distribution of a) Au-on-ZTO and b) bare ZTO without Au NP at an illumination of 520 nm using FDTD.

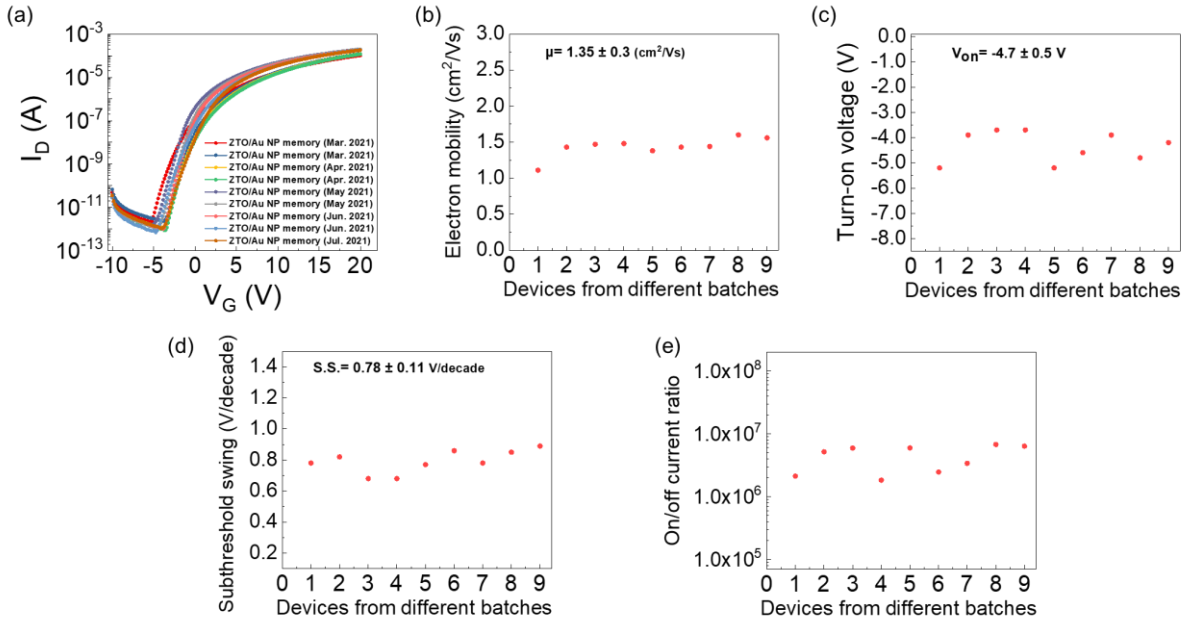

Figure S8. (a) I_D-V_G curves of ZTO/Au NP photomemory devices of different batches. (b)-(e) Statistical analysis of electron mobility, V_{on}, S.S., and on/off current ratio for the ZTO/Au NP photomemory devices.

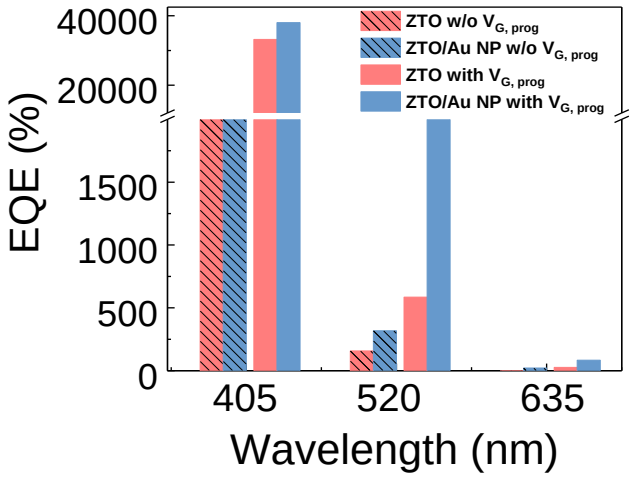

Figure S9. The dependence of EQE of the ZTO TFT and ZTO/Au NP photomemory on the wavelengths, with or without programming gate bias.

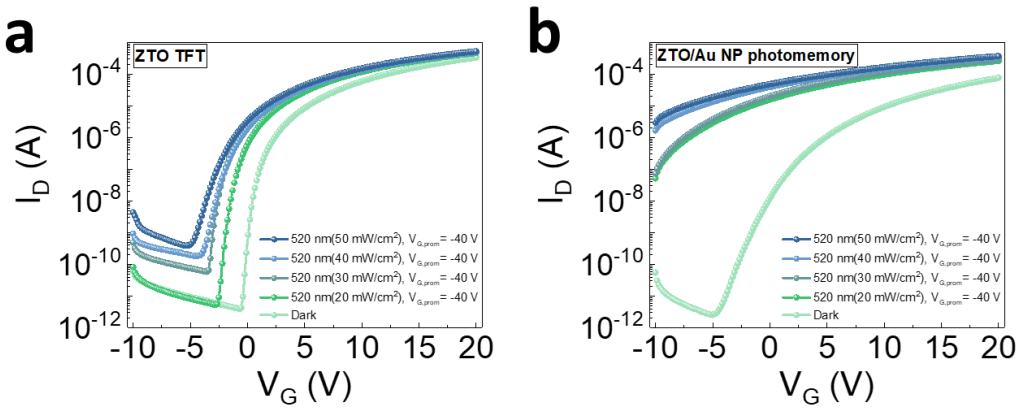

Figure S10. I_D-V_G transfer characteristics of a) ZTO TFT and b) ZTO/Au NP photomemory measured in dark or under light illumination at wavelength of 520 nm with different power densities, after a light-bias programming for 30 s at $V_{G,\,prog}$ = –40 V with light illumination of the associated wavelength.

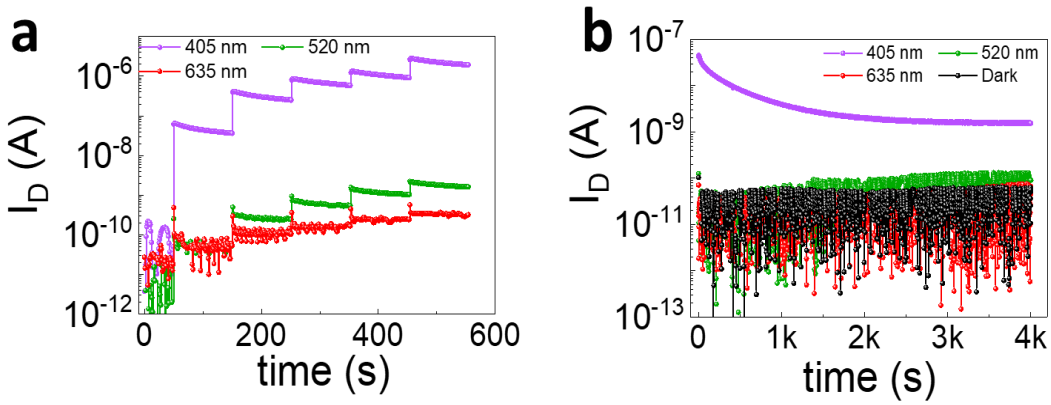

Figure S11. a) Multilevel data storage and b) retention of ZTO TFT after the light-bias application at various wavelengths for 1 s. All the readout states of ZTO TFT were measured at V_G = 0 V and V_D = 10 V.

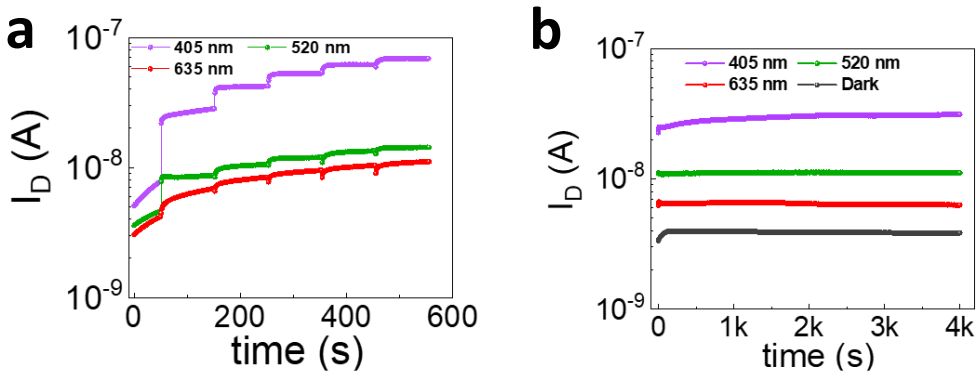

Figure S12. a) Multilevel data storage and b) retention of ZTO/Au NP photomemory after photoprogramming process at different wavelengths for 1 s. All the readout states and retention of ZTO/Au NP photomemory were measured at V_G = 0 V and V_D = 10 V.

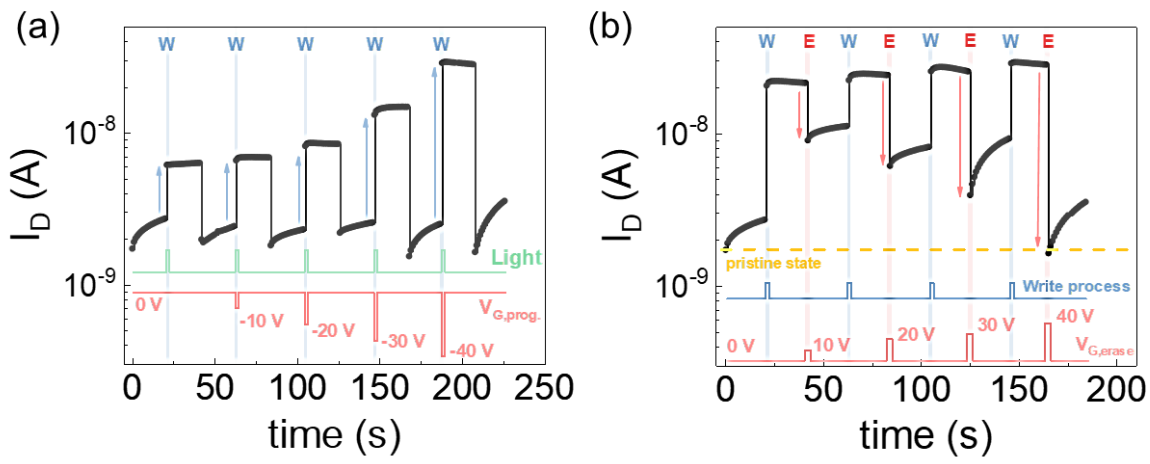

Figure S13(a) The current states of ZTO/Au NP photomemory using different light-bias co-stimulation programming processes with V_G = 0, –10, –20, –30, and –40 V under 520 nm light illumination for 1 s. (b) The current states of ZTO/Au NP photomemory using the different erasing processes with V_G = 10, 20, 30, 40 V for 2 s. All the current states are read at V_G = 0 V and V_D = 10 V for 20 s.

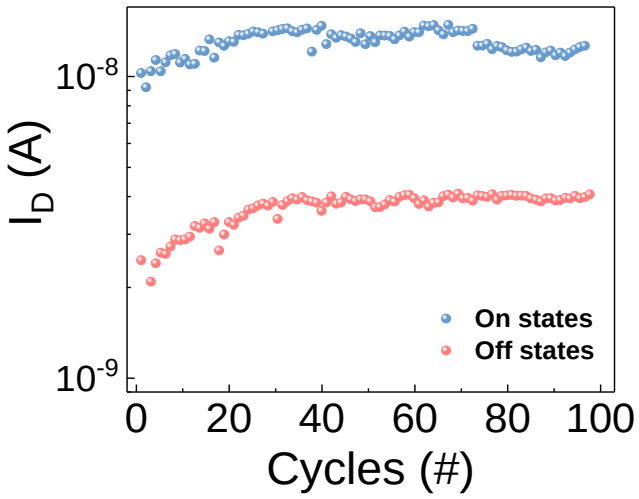

Figure S14. WRER switching cycle of ZTO/Au NP photomemory obtained using the 520 nm light and V_G = –40 V for 1 s as the programming (i.e., writing) process, and a $V_{G,erase}$ = 10 V for 1.5 s as the erasing process. The current states were measured at V_G = 0 V and V_D = 10 V.

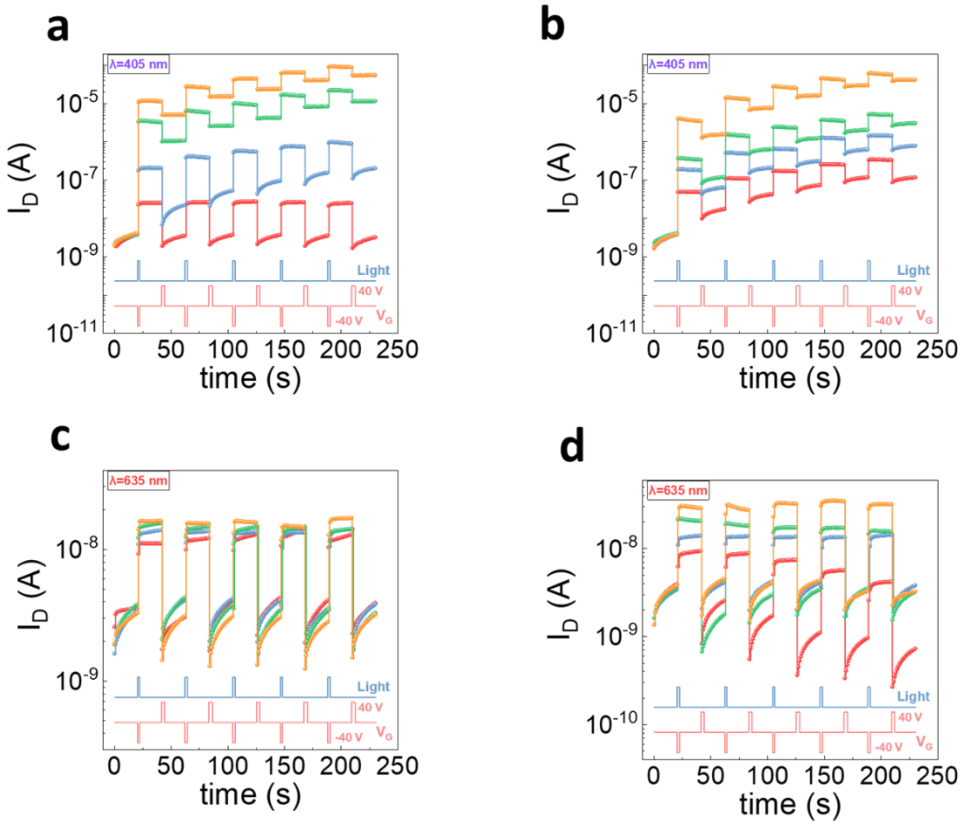

Figure S15. WRER switching cycle of ZTO/Au NP photomemory obtained using the light-bias application as the programming process and a V_G = 40 V for 2 s as the erasing process. a) WRER switching cycle using different light power densities for 1 s as the programming process (λ = 405 nm. Orange line: 4 mW/cm^2, green line: 3 mW/cm^2, blue line: 2 mW/cm^2, and red line: 1 mW/cm^2). b) WRER switching cycle using different programming times as the programming process (λ = 405 nm. Orange line: 5 s, green line: 2 s, blue line: 1 s, and red line: 0.5s. c) WRER switching cycle using different light power densities for 1 s as the programming process (λ = 635 nm. Orange line: 90 mW/cm^2, green line: 80 mW/cm^2, blue line: 70 mW/cm^2, and red line: 60 mW/cm^2). d) WRER switching cycle using different programming times as the programming process (λ = 635 nm. Orange line: 5 s, green line: 2 s, blue line: 1 s, and red line: 0.5s). All the current states of ZTO/Au NP photomemory device were measured at V_G = 0 V and V_D = 10 V.

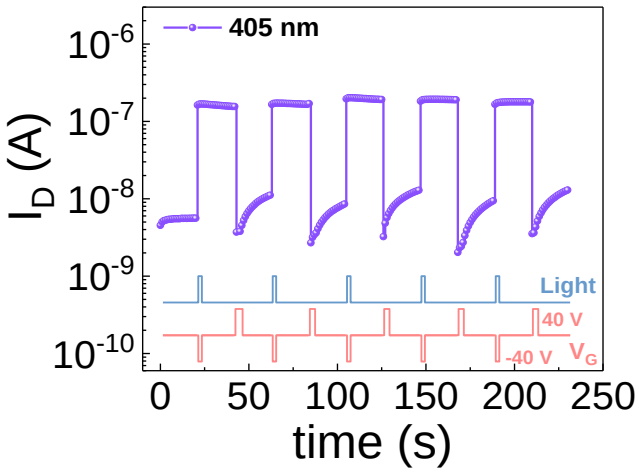

Figure S16. WRER switching cycle of ZTO/Au NP photomemory obtained using the 405 nm light (ρ = 2 mW/cm^2) and V_G = -40 V for 1 s as the programming process, and a V_G = 40 V for 10 s as the erasing process.

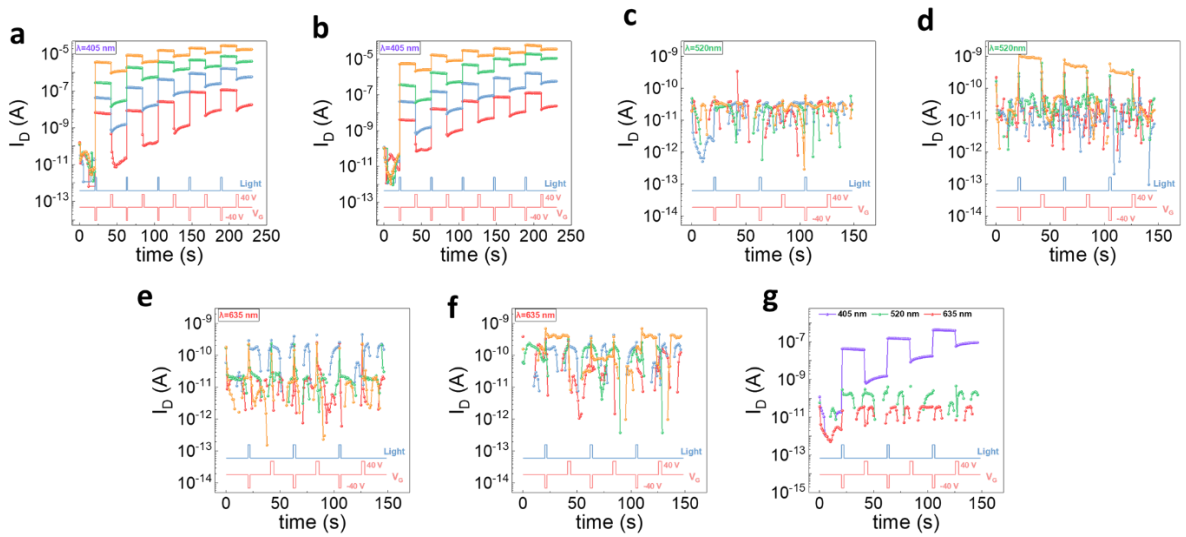

Figure S17. WRER switching cycle of ZTO TFT obtained using the light-bias application as the programming process and a V_G = 40 V for 2 s as the erasing process. a) WRER switching cycle using different light power densities for 1 s as the programming process (λ = 405 nm. Orange line: 4 mW/cm^2, green line: 3 mW/cm^2, blue line: 2 mW/cm^2, and red line: 1 mW/cm^2). b) WRER switching cycle using different programming times as the programming process (λ = 405 nm. Orange line: 5 s, green line: 2 s, blue line: 1 s, and red line: 0.5 s). c) WRER switching cycle using different light power densities for 1 s as the programming process (λ = 520 nm. Orange line: 50 mW/cm^2, green line: 40 mW/cm^2, blue line: 30 mW/cm^2, and red line: 20 mW/cm^2). d) WRER switching cycle using different programming times as the programming process (λ = 520 nm. Orange line: 5 s, green line: 2 s, blue line: 1 s, and red line: 0.5s). e) WRER switching cycle using different light power densities for 1 s as the programming process (λ = 635 nm. Orange line: 90 mW/cm^2, green line: 80 mW/cm^2, blue line: 70 mW/cm^2, and red line: 60 mW/cm^2). f) WRER switching cycle using different programming times as the programming process (λ = 635 nm. Orange line: 5 s, green line: 2 s, blue line: 1 s, and red line: 0.5s). g) WRER switching cycle using various wavelengths for 1 s as the programming process. All the current states of ZTO TFT device were measured at V_G = 0 V and V_D = 10 V.

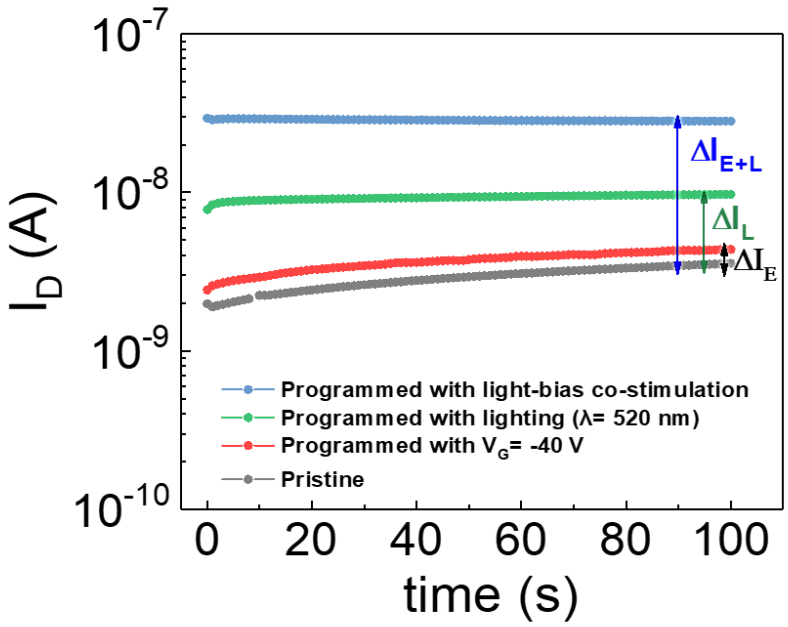

Figure S18. The current states of ZTO/Au NP photomemory after the gate bias (V_G = -40 V), lighting with λ = 520 nm (ρ = 30 mW/cm^2), and light-bias application for 1 s. All states are read at V_G = 0 V and V_D = 10 V.

Table S1. Comparison of the electrical characteristics including electron mobility, V_{on}, S.S., and on/off current ratio of ZTO/Au NP photomemory devices from different batches. (See Figure S8).

Device number	Electron mobility [cm^2/Vs]	Turn-on voltage [V]	Subthreshold swing [V/decade]	On/off current ratio
ZTO/Au NP memory (Mar. 2021)	1.11	-5.20	0.78	2.12×10^6
ZTO/Au NP memory (Mar. 2021)	1.43	-4.00	0.82	1.83×10^6
ZTO/Au NP memory (Apr. 2021)	1.47	-3.85	0.68	3.39×10^6
ZTO/Au NP memory (Apr. 2021)	1.48	-3.85	0.68	3.46×10^6
ZTO/Au NP memory (May 2021)	1.38	-5.20	0.77	5.96×10^6
ZTO/Au NP memory (May 2021)	1.43	-4.75	0.86	6.36×10^6
ZTO/Au NP memory (Jun. 2021)	1.44	-4.00	0.78	5.93×10^6
ZTO/Au NP memory (Jun. 2021)	1.60	-4.75	0.85	6.76×10^6
ZTO/Au NP memory (Jul. 2021)	1.56	-4.30	0.89	5.16×10^6

Table S2. The comparison of the photomemory performances.

Material	Wavelength [nm]	Programming time [s]	Retention [s]	Endurance	Multilevel performance
In_2O_3[1]	UV	5	10^4	-	8-bits
perovskite/CNTs heterojunction[2]	470	1	10^3	5 cycles	2-bits
CdS NRs[3]	White light	10	~10^4	6 cycles	-
BPE-PDI/SoI-PDI[4]	405, 530, 630	3	10^4	5 cycles	1-bit
IDTBT/ $Cs_2AgBiBr_6$@OS[5]	430, 450, 650	60	10^4	20 cycles	1-bit
Pentacene/ $Cs_2Pb(SCN)_2Br_2$[6]	450, 650	60	10^4	10 cycles	-
ZTO/Au NP **[this work]**	405, 520, 635	0.5	10^4	100 cycles	3-bits

References

1 S. Abbas, M. Kumar, D.-K. Ban, J.-H. Yun and J. Kim, *ACS Appl. Electron. Mater.*, 2019, **1**, 437-443.

2 Y. T. Li, L. Ding, J. Z. Li, J. Kang, D. H. Li, L. Ren, Z. Y. Ju, M. X. Sun, J. Q. Ma, Y. Tian, G. Y. Gou, D. Xie, H. Tian, Y. Yang, L. W. Wang, L. M. Peng and T. L. Ren, *ACS Cent. Sci.*, 2019, **5**, 1857-1865.

3 Z. Shao, T. Jiang, X. Zhang, X. Zhang, X. Wu, F. Xia, S. Xiong, S. T. Lee and J. Jie, *Nat. Commun.*, 2019, **10**, 1294.

4 Y. C. Chiang, C. C. Hung, Y. C. Lin, Y. C. Chiu, T. Isono, T. Satoh and W. C. Chen, *Adv. Mater.*, 2020, **32**, 2002638.

5 W. Lin, G. Chen, E. Li, L. He, W. Yu, G. Peng, H. Chen and T. Guo, *ACS Appl. Mater. Interfaces*, 2020, **12**, 43967-43975.

6 M. Y. Liao, Y. C. Chiang, C. H. Chen, W. C. Chen and C. C. Chueh, *ACS Appl. Mater. Interfaces*, 2020, **12**, 36398-36408.